Tunable Guided-mode resonance filter using Spacetime Periodic Structure

Yaser Khorrami
dept. electrical&computer engineering
Tarbiat Modares University
Tehran, IRAN
y.khorrami@modares.ac.ir

Davood Fathi
dept. electrical&computer engineering
Tarbiat Modares University
Tehran, IRAN
d.fathi@modares.ac.ir

Nasrin Razmjooei
dept. electrical engineering
University of Texas at Arlington
Texas, USA
nasrin.razmjooei@uta.edu

Raymond C. Rumpf
dept. electrical&computer engineering
University of Texas at El Paso
Texas, USA
rcrumpf@utep.edu

Abstract*— We present a tunable planar guided-mode resonance (GMR) filter using time-varying permittivity along grating nanobars. Results show that the effective medium concept in the temporal state is exactly the same as the spatial state. Furthermore, the structure has spatial periodicity to save the resonance peak of the passive GMR in addition to the temporal periodicity that is used to tune the resonance location around the static reflection and transmission resonance peak as blueshift or redshift. Moreover, the proposed 1D+1 spacetime GMR filter has a broader bandwidth (BW) for blueshift in comparison to the redshift of the peak resonance.

Keywords—Spacetime, grating, tunable, filter.

I. Introduction

According to the grating's inverse design of the flowchart presented in Ref. [1], we have shown the process of designing a passive one-dimensional (1D) grating in Fig. 1. The schematic of the two-layer structure has been shown in inset of Fig. 1 (a). The permittivity and thickness of the upper and lower layers are (ε_1, d_1) and (ε_2, d_2), respectively. By selecting the wavelength of 1.5 μm (for incident wavelength) and $\varepsilon_2 = 2.35$ and employing nonlinear least-squares optimization (LSO) method, the desired variables of ε_1, d_1 and d_2 can be found as 2.1, 81 nm and 910 nm, respectively. Initial estimation estimationsfor these parameters is 2, 100 nm and 700 nm. The reflection and transmission spectra of the two-layer structure have been depicted in Fig. 1 utilizing the in-house developed simulator based on transfer matrix method (TMM) [2]. The logarithmic convergence diagram for the LSO approach is depicted in the inset plot of Fig. 1(a), which converges to 1.50387e-08 after 130 iterations in 5 seconds. After reaching the optimized parameters, using the effective medium theory (EMT) of $f = (\varepsilon_1 - \varepsilon_{\text{inc}})/(\varepsilon_2 - \varepsilon_{\text{inc}})$ for incident electric field perpendicular to the grating vector (TE polarization), the duty cycle (fill factor) can be calculated as $f = 0.82$. Fig. 1 (b) shows the narrowband reflection and transmission spectra of the designed 1D grating with 1.5 μm resonance wavelength which are plotted using in-house developed simulator based on rigorous coupled wave analysis (RCWA) method [3-4]. As demonstrated in the inset schematic of Fig.1(b) depth of grating is 81nm, depth of substrate is 910nm, and the permittivity of the entire structure, surrounded by air, is 2.35.

II. Implementation

In the following, we aim to design an active device, by extending the modeled GMR depicted in Fig. 1. Figure 2 represents the spatiotemporally GMR with spatial periodicity along x-axis and temporal variation along y-axis. Temporal modulation of the permittivity can be achieved using electrical bias (or radio frequency excitation) to alter the density of the injected carrier into the bars [5-6].

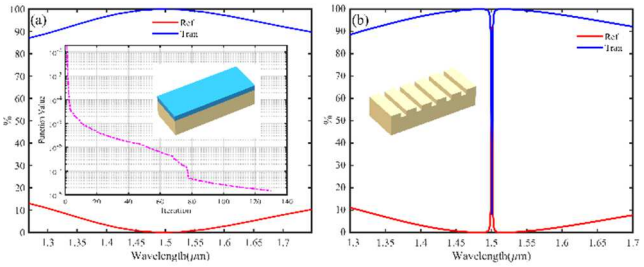

Fig. 1. Reflection and transmission spectra versus wavelength using (a) TMM. The inset figure shows the logarithmic convergence diagram versus the iteration number applying the LSO method. The inset schematic is the two-layer structure. (b) RCWA method. The inset shows the designed GMR with unique permittivity for the whole structure.

The contacts on the bars are used to show how the wires are connected to the intrinsic bars via blue and red parts that operate as p-type and n-type gates, respectively. To prevent any carrier leakage from grating layer to the substrate, a thin transparent layer made of a different material, such as a transparent conducting oxides (ITO), can be placed between the grating and substrate layers [7-11].

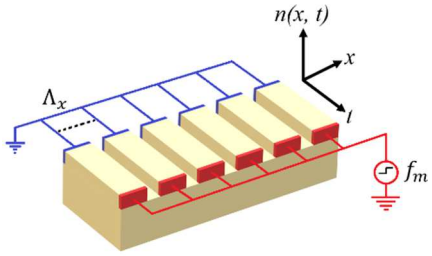

Fig. 2. 1D+1 Spacetime-gradient two-layer GMR filter with frequency modulation along t-axis.

In Fig. 2, for the incident wavelength of 1.5 μm, the spatial periodicity is $\Lambda_x = 1.315\ \mu m$ with duty cycle of 82%, the depth of grating layer is 81nm, and the depth of substrate layer is 910nm. In active state, the polarization is set to TE as it is in the passive designed state. Number of grids along x and y-axis is set to be 500. For spacetime simulation, we employ an in-house developed simulator based on the spacetime Fourier modal method (ST-FMM) [6]. Both the spatial diffraction order and temporal harmonic index are set to be 11.

978-1-6654-7899-1/22/$31.00 ©2022 IEEE

III. Results and Disscussion

For implementing the time-variation, we assume the variation of the refractive index in the form of step function. Temporal multistep can be generated by modulation depth of $\delta = 0.1489$ and modulation frequency of $f_m = 0.03f_0$ over static permittivity of 2.35. Therefore, we have high and low permittivity values equal to the 2.7 and 2.0 with temporal period of $\Lambda_t = 1/f_m = 16.67\text{e}-14$. Fig. 3 shows the reflection and transmission spectra for the temporal duty cycle of 0.1 and 0.9 along t-axis (or y-axis) which is shown by f_y. The left inset in Fig. 3(a) and the right inset in Fig. 3(b) demonstrate the unit cell for spatial period of Λ_x= 1.315 μm with duty cycle of 82% and temporal period of Λ_t= $1/f_m$ = $16.67\text{e}-14$, considering temporal duty cycle equal to 0.1 and 0.9, respectively.

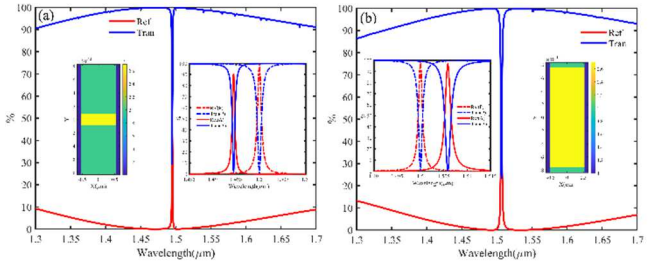

Fig. 3. Temporaly modulated GMR filter using step function time-varying permittivity along t-axis for (a) red-shift resonance peak, $f_y = 0.1$ and (b) blue-shift resonance peak, $f_y = 0.9$. The permittivity has variation between 2 and 2.7, with $f_m = 0.03f_0$ and $\delta = 0.1489$. The static permittivity is 2.35.

Fig. 3(a) shows the shift of the passive resonance peak to the lower wavelength. The passive resonance has been illustrated in the right inset of Fig. 3(a) with dashed-dotted line in 1.5 μm and the redshift with solid line which has the resonance peak in 1.4944 μm with bandwidth of (FWHM) 5.7273e-10. For passive state in peak at 1.5 μm, BW is equal to 9.4949e-10. Fig. 3(b) shows resonance peak of the temporal GMR which has experienced a blueshift. The blueshift resonance peak in 1.5058 μm with BW of 1.3384e-09 for solid lines is represented in the left inset of Fig. 3(b).

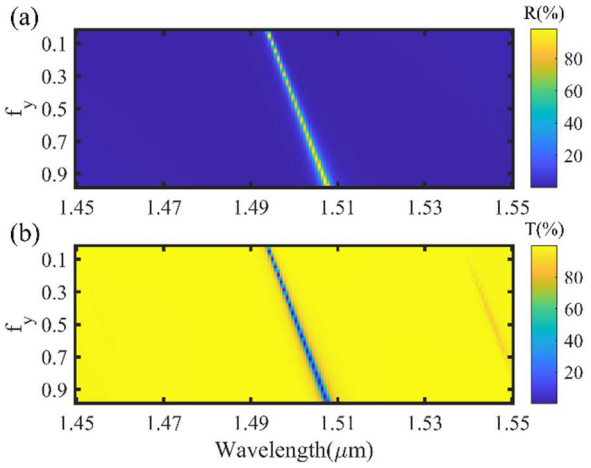

Fig. 4. Contour plots of the (a) reflection and (b) transmission magnitude of temporal GMR filter versus the time-variation fill fraction of f_y and the incident wavelength.

In both spectrum of insets in Fig. 3, we have shown the passive and active state with P and A in the parenthesis, respectively. Now, we use effective permittivity to consider passive equivalent state for each temporally one. From $\varepsilon_{eff} = f_y\varepsilon_{max} + (1-f_y)\varepsilon_{min}$, we have $\varepsilon_{eff} = 2.07$ and 2.63, for temporally GMRs with $f_y = 0.1$ and $f_y = 0.9$, respectively. Simulation shows the exact similarity of the passive designed GMR using effective permittivity theory and the results from temporally designed GMR in Fig. 3.

Fig. 4 shows the contour plots of reflection and transmission magnitude versus fill fraction of time periodicity along y-axis and the incident wavelength to the grating layer. As can be observed, for $f_y < 0.5$, red shift occurs in resonance peak of the GMR, while for $f_y > 0.5$, the blueshift in the resonance take place. Fig. 4(a) shows that for smaller amount of the temporal duty cycle, the discontinuities between the resonant wavelengths are more pronounced, but with increasing f_y, the same intensification peaks occur for different duty cycles (broadening on f_y). A similar behavior can be seen in Fig. 4(b). Another aspect illustrated in Figure 4 is that, according to effective permittivity theory, a higher duty cycle (or a longer time period of external radio frequency excitation) can enhance effective permittivity, resulting in a new GMR with higher permittivity and resonance. This shows that we can adjust our design in any multistep temporal pulse tuning. Broadening on wavelength is another phenomenon that resulted from Fig. 4 by increasing f_y, so that at higher duty cycles, the FWHM of the resonance is more broaden than at lower cycles.

References

[1] Y. Khorrami, D. Fathi, and R. C. Rumpf, "Guided-mode resonance filter optimal inverse design using one- and two-dimensional grating," J. Opt. Soc. Am. B, vol. 37, pp. 425-432, Jul. 2020.

[2] Y. Khorrami, D. Fathi, A. Khavasi, and R. C. Rumpf, "Passive and Active Slab Waveguide Mode Analysis Using Transfer Matrix Method," NUSOD-21 conference, Sep. 2021.

[3] R. Magnusson, K. J. Lee, H. Hemmati, P. Bootpakdeetam, J. Vasilyev, F. A. Simlan, N. Razmjooei, Y. H. Ko, S. Zhang, S. G. Lee, and H. G. Svavarsson, "Properties of resonant photonic lattices: Bloch mode dynamics, band flips, and applications," Proc. SPIE 11290, 1129006 March 2020.

[4] E. Jebellat, M. Baniassadi, A. Moshki, K. Wang, M. Baghani (2020) "Numerical investigation of smart auxetic three-dimensional metastructures based on shape memory polymers via topology optimization,", J Intell Mater Syst Struct 3, pp.1838–1852, Sep. 2020.

[5] J. h. Park, J.-H. Kang, S. J. Kim, X. Liu, and M. L. Brongersma, "Dynamic reflection phase and polarization control in metasurfaces," Nano Lett., vol. 17, pp. 407–413, Dec. 2017.

[6] H. Asadzadeh Sr., S. Renkes, M. J. Kim, and G. Alexandrakis, "Multi-physics simulations of label-free optical-electrical forces acting on a silica nanoparticle trapped in a SANE plasmonic nanopore," Proc. SPIE 11978, Plasmonics in Biology and Medicine XIX, 1197803 March 2022.

[7] Y. W. Huang et al., "Gate-tunable conducting oxide metasurfaces," Nano Lett, vol. 16, pp. 5319–5325, Aug. 2016.

[8] J. Park, J.-H. Kang, X. Liu, and M. L. Brongersma, "Electrically tunable epsilon-near-zero (ENZ) meta film absorbers," Sci. Rep., vol. 5, pp. 15754, Sep. 2015.

[9] E. Feigenbaum, K. Diest, and H. A. Atwater, "Unity-order index change in transparent conducting oxides at visible frequencies," Nano Lett., vol. 10, pp. 2111–2116, May. 2010.

[10] J. W. Cleary, E. M. Smith, K. D. Leedy, G. Grzybowski, and J. Guo, "Optical and electrical properties of ultra-thin indium tin oxide nanofilms on silicon for infrared photonics," Opt. Mater. Exp., vol. 8, pp. 1231–1245, May. 2018.

[11] M. M. Salary and H. Mosallaei, "Electrically tunable metamaterials based on multimaterial nanowires incorporating transparent conductive oxides," Sci. Rep., vol. 7, pp. 10055, Aug. 2017.